SUPPLEMENTARY MATERIAL

Myosin II activity softens cells in suspension
by C. J. Chan et al.

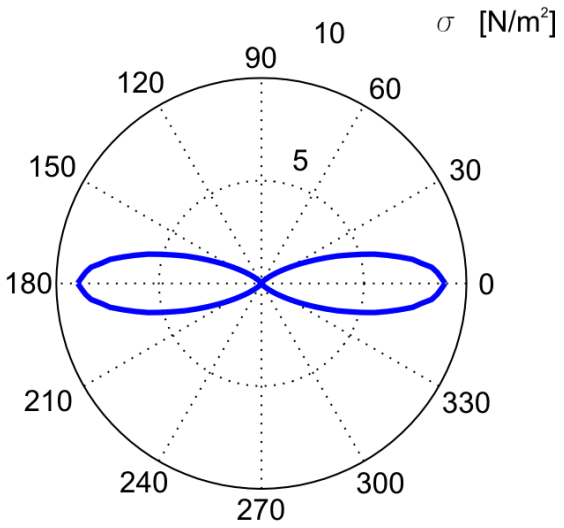

Fig. S1: Optically induced stress profile on a spherical object in an optical stretcher, calculated by generalised Lorenz-Mie theory. For these calculations, the object itself not shown in figure, the refractive index of the object was assumed to be $n = 1.365$, the cell size radius 11 µm, and the distance of the optical fibers from the cell 85 µm. The applied stretch power was 0.8 W per fiber.

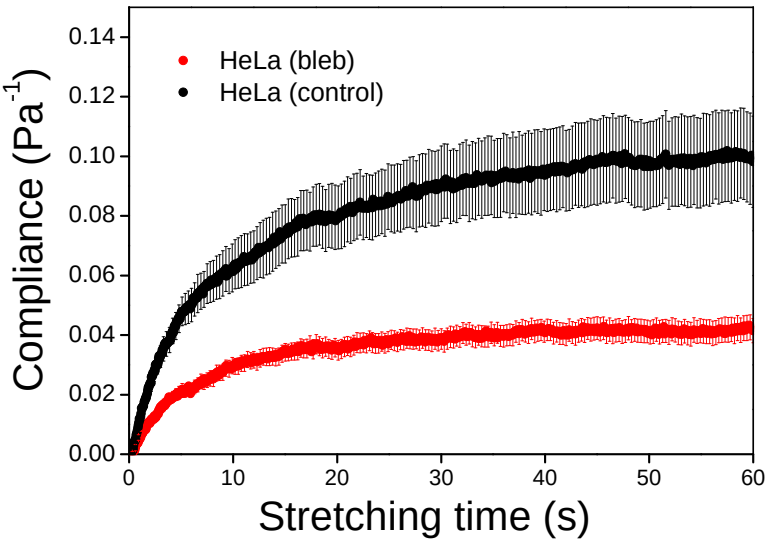

Fig. S2: Influence of blebbistatin on compliance of HeLa cells in suspension at long timescale. Compliance curves for HeLa cells after treatment with blebbistatin (n = 47), compared to controls (n = 20), when stretched for an extended period of 60 s.

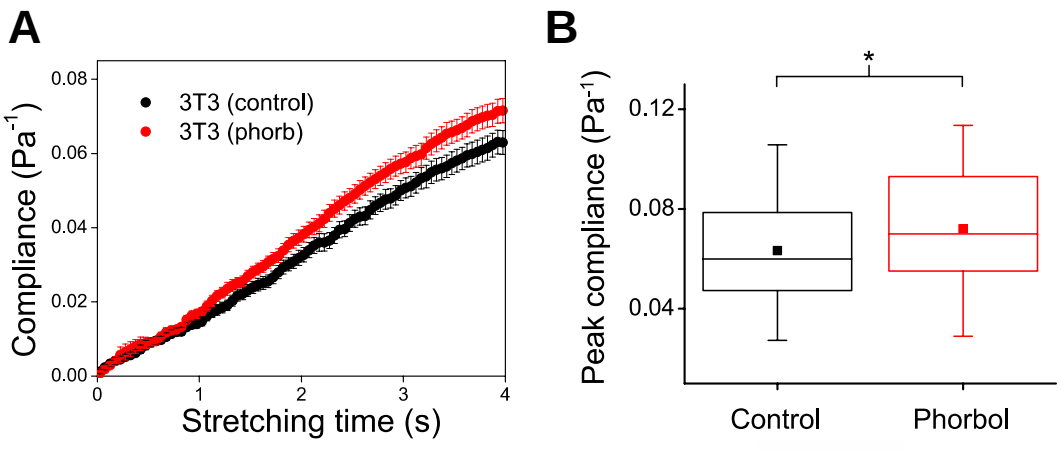

Fig. S3: Effect of enhancing myosin II activity on compliance of 3T3 fibroblasts in suspension. A. Compliance curves for 3T3 fibroblasts after treatment with phorbol 12,13-dibutyrate (n = 73), compared to controls (n = 65). **B.** Box plots of the peak compliance for controls versus phorbol 12,13-dibutyrate-treated cells. *$p < 0.05$.

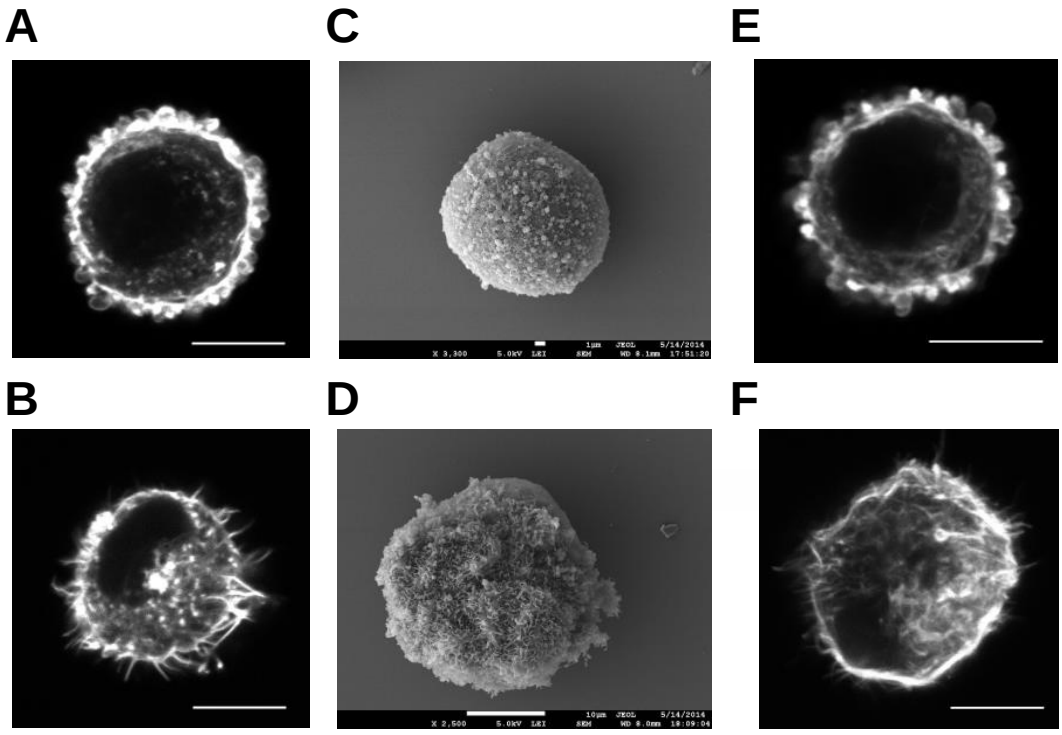

Fig. S4: Distinct morphological differences in actin cortical structures between untreated and myosin-inhibited 3T3 fibroblasts in suspension. A, B. Confocal images of a representative suspended untreated 3T3 fibroblast stained for actin (phalloidin-Alexa Fluor 488 dye), and another cell treated with blebbistatin, respectively. The untreated cells show a dense actin cortical layer underneath the plasma membrane with frequent formation of bleb-like structures, while the actin cortex of blebbistatin-treated cells show a more microvillous cell surface. **C, D.** SEM images of untreated and blebbistatin-treated suspended 3T3 fibroblasts, respectively. Similar differences in actin cortical structures on an ultrastructural level were

revealed. **E, F.** Confocal images of representative untreated cell stained for actin, and another cell treated with ML7 (another myosin II inhibitor), respectively. The distinct morphological change of cortical actin structures mirrors that observed for blebbistatin-treated cells. All scale bars are 10 μm.

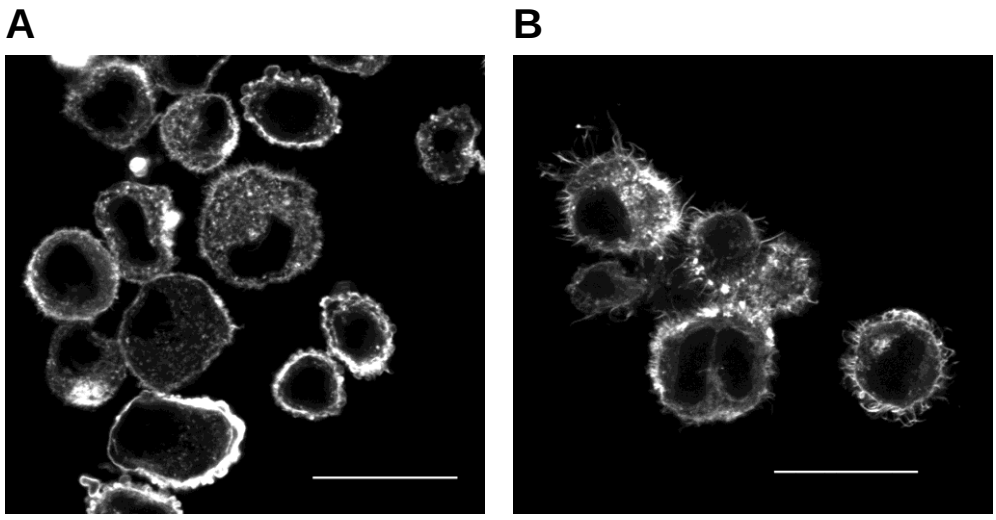

Fig. S5: A. Confocal image of trypsinized, untreated 3T3 fibroblasts stained for actin. **B.** Confocal image of actin-stained cells treated with blebbistatin. The distinct morphological differences in actin cortical structures is highly reproducible and observed across the entire cell population. Scale bars are 30 μm.

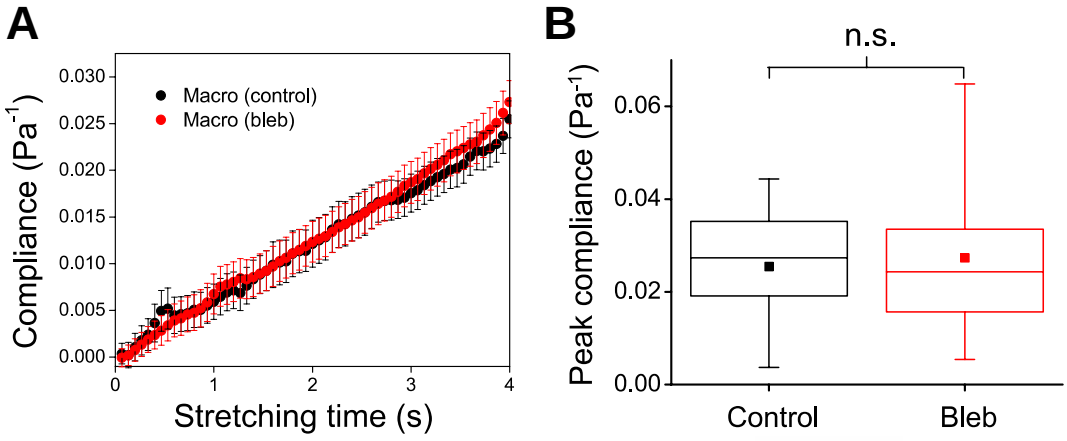

Fig. S6: Influence of blebbistatin on compliance of HL60-differentiated macrophages in suspension. A. Compliance curves of macrophages when treated with blebbistatin (n = 51), compared to controls (n = 52). **B.** Box plots of the peak compliance for controls versus blebbistatin-treated cells. There is no significant difference between the two populations.

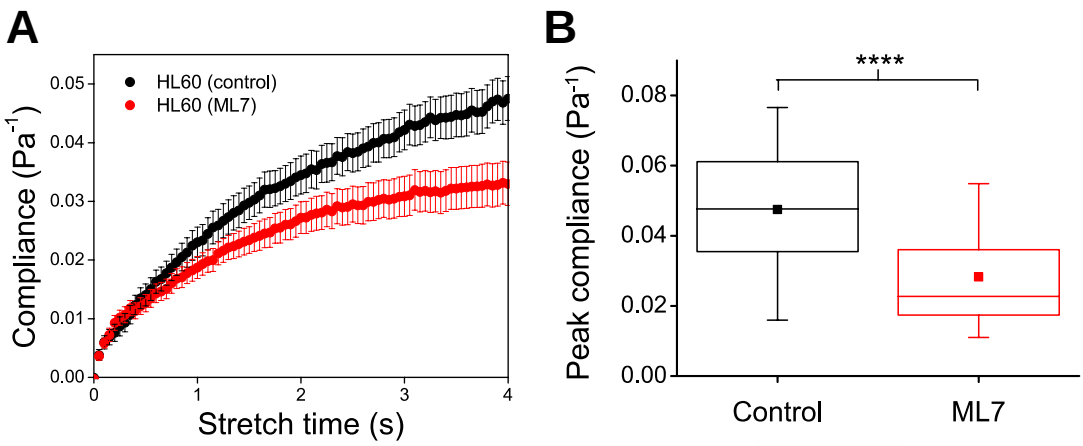

Fig. S7: Influence of ML7 on compliance of undifferentiated HL60 cells in suspension. A. Compliance curves for HL60 cells after treatment with ML7 (n = 36), compared to controls (n = 33). **B.** Box plots of the peak compliance for controls versus ML7-treated cells. ****$p < 0.0001$.

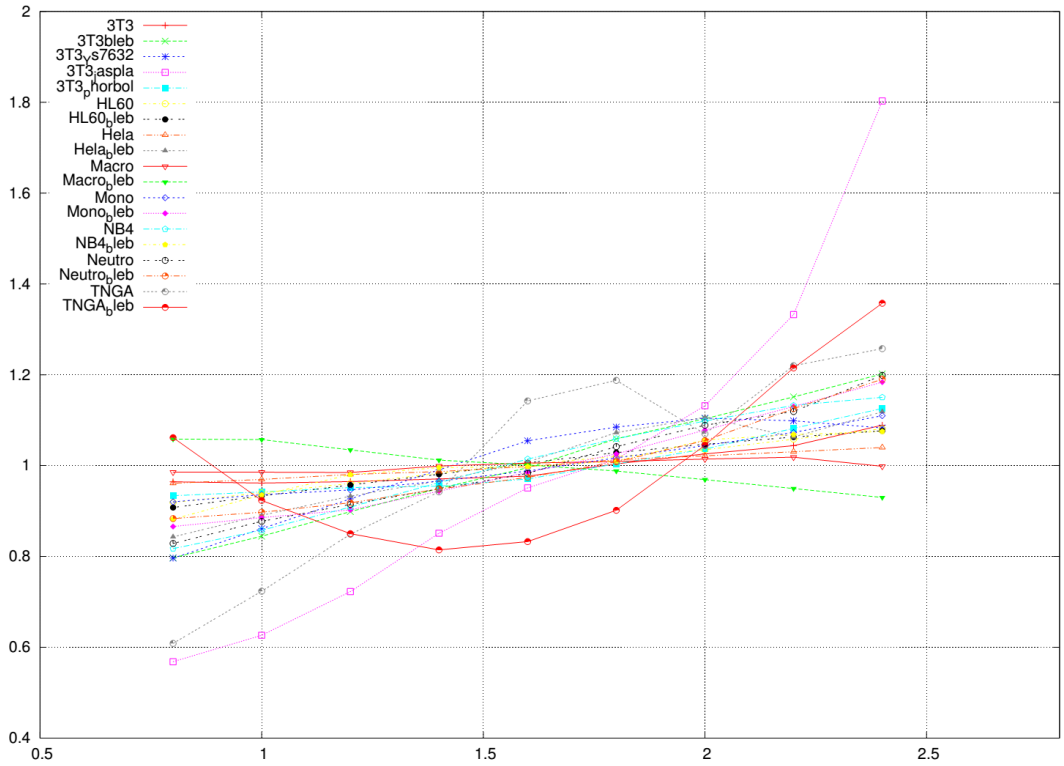

Fig. S8: Sensitivity analysis: Relative long time viscosity $\eta_s(t_c)/<\eta_s>$ as a function of cut-off-time t_c. For most cell lines η_s varies less than 10% for 1.1 s < t_c <2.2 s. For times larger than 2.5 s lack of data results in large errors. TNGA cells show a slightly larger dependence of the order 20%. Only 3T3 with Jasplakinolide shows relatively strong dependence on t_c.

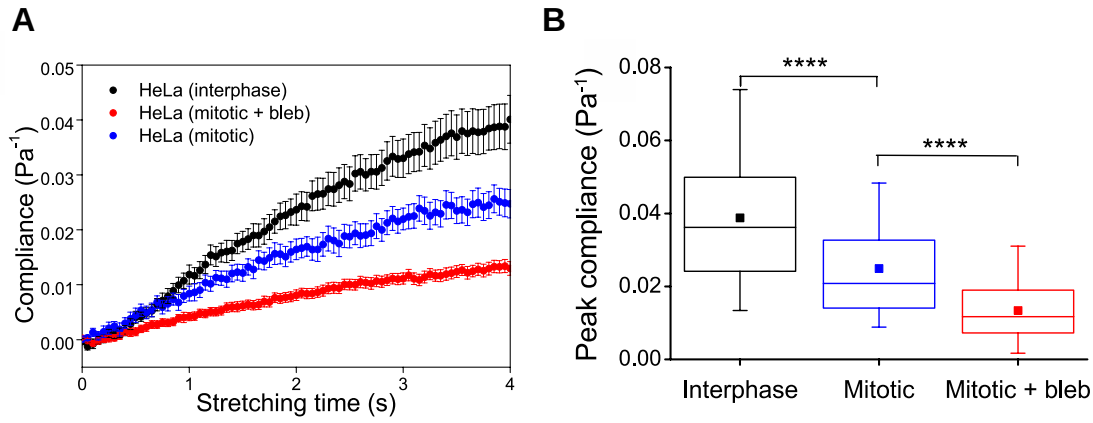

Fig. S9: Influence of blebbistatin on compliance of mitotic HeLa cells in suspension. A. Compliance curves for mitotic HeLa cells (n = 27) or mitotic cells treated with blebbistatin (n = 62), compared to interphase HeLa cells (n = 26). All experiments were performed on the same batch of synchronized cells. **B.** Box plots of the peak compliance for interphase HeLa cells compared to mitotic cells with and without blebbistatin. ****$p < 0.0001$.

Power law model	β
3T3 (control)	1.03 ± 0.02
3T3 (blebbistatin)	0.40 ± 0.01
3T3 (Y-27632)	0.48 ± 0.01
HeLa (control)	1.01 ± 0.02
HeLa (blebbistatin)	0.69 ± 0.03
TNGA (control)	0.83 ± 0.08
TNGA (blebbistatin)	0.24 ± 0.03

Table S1: Changes in cell fluidity for naturally adherent cells following inhibition of myosin II activity by blebbistatin or Y-27632. The power law exponents were extracted from fitting the power law model to the cell compliance curves for various cell lines (control vs. blebbistatin or Y-27632). The errors represent standard errors of the fitted parameters when computed within 95% confidence interval.

Standard linear liquid	η_s (*Pa.s*)	E_t (*Pa*)	η_t (*Pa.s*)	τ (*s*)
3T3 (control)	61.8 ± 0.8	1111.8 ± 791.3	93793.3 ± 725554.8	84.36 ± 650.71
3T3 (blebbistatin)	260.7 ± 6.4	45.0 ± 0.57	21.1 ± 0.76	0.47 ± 0.02
3T3 (Y-27632)	178.5 ± 2.1	40.3 ± 0.3	23.2 ± 0.5	0.58 ± 0.01
HeLa (control)	137.7 ± 1.0	1310.3 ± 257.4	7301.7 ± 4752.5	5.57 ± 3.46
HeLa (blebbistatin)	352.3 ± 14.7	153.2 ± 8.5	148.7 ± 10.0	0.97 ± 0.04
TNGA (control)	258.7 ± 19.3	97.5 ± 6.8	143.9 ± 17.3	1.48 ± 0.14
TNGA (blebbistatin)	654.8 ± 78.9	190.3 ± 16.5	15.2 ± 1.7	0.08 ± 0.01

Table S2: Changes in viscoelastic parameters of naturally adherent cells following myosin II inhibition by blebbistatin or Y-27632. Transient and steady-state viscoelastic parameters were extracted from fitting the SLL model to the compliance curves, for various cell lines (control vs. blebbistatin or Y-27632). The errors represent standard errors of the fitted parameters when computed within 95% confidence interval.

β	Control	Blebbistatin
NB4	0.51 ± 0.01	0.48 ± 0.01
HL60	0.81 ± 0.01	0.77 ± 0.01
Neutrophil	0.57 ± 0.01	0.84 ± 0.03
Monocytes	0.87 ± 0.02	0.55 ± 0.01

Table S3: Changes in cell fluidity for naturally suspended cells following inhibition of myosin II activity by blebbistatin. The power law exponents were extracted from fitting the power law model to the compliance curves, for controls and cells treated with blebbistatin. The errors represent standard errors of the fitted parameters when computed within 95% confidence interval.

Standard linear liquid	η_s (*Pa.s*)	E_t (*Pa*)	η_t (*Pa.s*)	τ (*s*)
NB4 (control)	204.8 ± 2.1	60.2 ± 0.5	42.3 ± 1.2	0.70 ± 0.02
NB4 (blebbistatin)	396.7 ± 7.0	122.5 ± 2.0	63.5 ± 1.3	0.52 ± 0.01
HL60 (control)	114.6 ± 1.1	126.5 ± 3.9	120.0 ± 5.1	0.95 ± 0.03
HL60 (blebbistatin)	183.2 ± 1.6	164.1 ± 3.9	140.0 ± 4.4	0.85 ± 0.02
Neutrophil (control)	88.3 ± 3.5	28.8 ± 1.1	18.0 ± 0.9	0.62 ± 0.02
Neutrophil (blebbistatin)	115.7 ± 3.2	115.6 ± 9.8	118.5 ± 14.4	1.03 ± 0.09
Monocytes (control)	74.9 ± 1.05	93.3 ± 5.0	111.2 ± 8.5	1.19 ± 0.07
Monocytes (blebbistatin)	151.7 ± 3.7	53.5 ± 1.37	30.4 ± 1.2	0.57 ± 0.02

Table S4: Changes in viscoelastic parameters of naturally suspended cells following myosin II inhibition by blebbistatin. Transient and steady-state viscoelastic parameters were extracted from fitting the SLL model to the compliance curves, for various cell lines (control vs. blebbistatin). The errors represent standard errors of the fitted parameters when computed within 95% confidence interval.

Movie S1. Advection of HL60s through a microfluidic microcirculation mimetic with constriction width of 5 µm. Blebbistatin-treated HL60 cells require significantly longer times to deform before they can slip through the constrictions, as compared to the untreated cells when tested at the same driving pressure of 50 mbar. Video presented is in real time. (WMV)